A comparative study of electron and positron scattering from molecules. IV. CH_3Cl, CH_3Br, and CH_3I molecules

M. Kimura, O. Sueoka, C. Makochekanwa, H. Kawate, and M. Kawada
Graduate School of Science and Engineering, Yamaguchi University, Ube, Yamaguchi 755-8611, Japan

(Received 5 February 2001; accepted 24 July 2001)

An experimental study of electron and positron scattering from CH_3Cl, CH_3Br, and CH_3I molecules has been carried out, and total cross sections (TCSs) for both projectiles were determined. Several strong structures due to resonances in the TCSs have been observed for electron impact, while weak but not negligible structures have also been seen for positron impact. A strong variation for the dominant resonance peak seen at around 10 eV was found to depend on a type of halogen atoms, and a detailed study of this dependence on molecular species has been performed to understand the origin and nature of these resonances. The continuum multiple-scattering method has been employed for the analysis of experimental results in addition to the evaluation of the elastic cross section. For larger halogen atoms, TCSs tend to possess larger magnitudes at energies above 100 eV than for smaller halogen atoms suggesting that the halogen atoms in fact dominate the dynamics, and their magnitudes increase in the order of $CH_3I > CH_3Br > CH_3Cl$. A comparative study of CH_4 was also performed to provide insight on the effects of molecular geometrical structure and electronic state. © *2001 American Institute of Physics.* [DOI: 10.1063/1.1402996]

I. INTRODUCTION

Electron impact on various types of halogen-substituted methanes (CH_3Cl, CH_3Br, and CH_3I) offers an interesting opportunity for a comparative study of a great deal of temporary anion states and corresponding molecular structures.[1] For a given molecular target, by comparing scattering processes for electron and positron collisions, much information on the interactions and dynamics including resonances that provide a deeper understanding of basic physics and chemistry can be extracted.[2] Although positron attachment has not been clearly observed, nor experimentally confirmed yet, it is extremely interesting to study a positron attachment process in connection with that of electron attachment through which the dissociation mechanism of molecules via attachment can be examined. In electron attachment to molecules, a majority of molecular negative ions are unstable and eventually undergo fragmentation. The resulting fragment molecular species should be different for electrons and positrons, and if this is the case, they may then be used for the selective production of specific fragments. Therefore, we have conducted a comparative study of electron and positron scattering from CH_3Cl, CH_3Br, and CH_3I molecules for total and elastic cross sections to provide benchmark data. Since no comprehensive data for these molecules are available, the present results by these projectiles would be useful and would provide a basic guideline for the compilation of cross section data sets. They may also give a clue for identifying the fingerprint of positron attachment.[3]

Furthermore, we carry out a comparative study of total cross sections (TCSs) for CH_4 and those of CH_3Cl, CH_3Br, and CH_3I, so that we can contrast the effect of the electron distribution of halogen atoms, their bond lengths, and other properties on the TCSs. Our current study provides more detailed information on total and elastic cross sections for the molecules as well as basic information on molecular structures, and encourages further experimental and theoretical studies for individual scattering processes to obtain a complete understanding of the physical and chemical properties of these molecules.

There have been several experimental attempts to investigate electron impact on these molecules. Among these, Krzysztofowicz and Szmytkowski,[4–6] Benitez *et al.*,[7] and Karwasz *et al.*[8] have measured TCSs for electron impact in nearly overlapping energy regions. Hence, it is interesting to compare the present results with these earlier measurements. Vallance *et al.*[9] have carried out an experimental study for electron impact ionization of these molecules, and their results, along with the present results, should comprise important components of the complete data set we need.

Based on transmission spectroscopy, Barrow's group[10] has investigated transient negative-ion formation processes of these molecules below a few eV. This study should provide useful and important information for identifying the origin of resonances and electronic structures. Their conclusions are helpful for further laying the ground for the understanding of positron attachment.

Some relevant molecular properties including dipole moments, ionization potentials and bond lengths for these molecules are listed in Table I.

II. EXPERIMENTAL AND THEORETICAL METHODS

A. Experiment

The linear transmission method has been used to measure the absolute TCS for positron and electron scattering from halogenized methanes (CH_3Cl, CH_3Br, and CH_3I). In the present experiments we have used the same apparatus as in our previous TCS measurements[11] and only some specific

TABLE I. Dipole moments, ionization potentials, and bond lengths.[a]

Molecules	Dipole moment (Debye)	IP (eV)	Bond length (Å) C–H	Bond length (Å) C–X
CH_3F	1.858	12.47	1.095	1.382
CH_3Cl	1.892	11.22	1.0854	1.7760
CH_3Br	1.822	10.54	1.0823	1.9340
CH_3I	1.62	9.538	1.084	2.132

[a]Reference 30.

features will be summarized here. A schematic diagram of the experimental apparatus is presented in Fig. 1. The slow positrons are produced by moderation of fast positrons from a 65–85 μCi ^{22}Na radioisotope through an annealed tungsten ribbon moderator. The energy width of the beam is about 1.5 eV. These positrons are accelerated by an electrostatic field applied from a potential at the moderator. The positrons that passed through the collision cell are transported into the detector by the magnetic field. A retarding potential unit located at the front of the detector expels the inelastically scattered positrons, so that only the elastically scattered positrons are detected. The positron-beam intensity is measured by its flight time between the moderator and the detector and accumulated as a time-of-flight spectrum. For electron scattering, the slow electrons are produced after secondary electrons from the isotope source are moderated by multiple scattering in the tungsten moderator. The electron beam has an energy spread of ~1 eV. The measurement of TCSs is performed within the energy range 0.7–600 eV for positrons and 0.8–600 eV for electrons.

The TCS values Q_t are derived from

$$Q_t = -\frac{1}{nl}\ln\left(\frac{I_g}{I_v}\right),$$

where I_g and I_v correspond to the projectile beam intensities transmitted through the collision cell with and without the target gas of number density n, respectively. The effective length l of the collision cell was established by normalizing the TCSs to those of the positron-N_2 data of Hoffman *et al.*[12] We confirmed the pressure independence of the TCS of CH_3X by electron scattering experiments at selected energies (6 eV and 27 eV) within the present energy range.

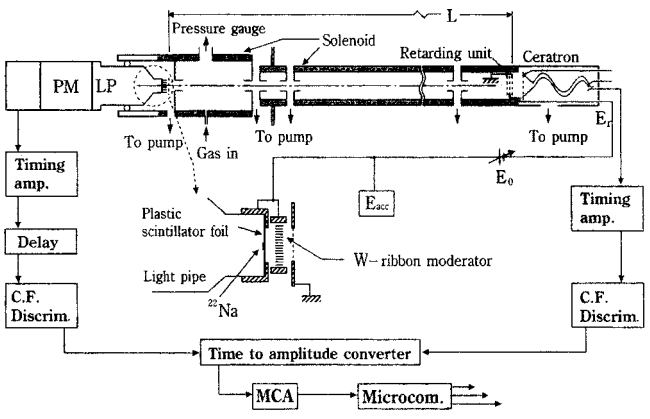

FIG. 1. A schematic diagram of the experimental apparatus.

In the present experiment, due to the magnetic field and a large collision cell aperture, the detector can also detect positrons or electrons scattered into small angles around the forward direction. In order to derive TCSs accurately for both positron and electron scattering, it is necessary to make a correction to account for this effect. To do so, we take the geometry, the external magnetic field and the differential cross section data from the theoretical results of the paper into account, using a procedure described in detail previously.[13] The correction for electron scattering amounts to 10–18% below 30 eV, but becomes much smaller at higher energies, down to <5% above 100 eV. For positron scattering, the corrections are generally found to be slightly larger than those for electron scattering.

The sum of all uncertainties was estimated to be 3–5% and 4.5–6.5% for electron and positron scattering, respectively. The contributions from the beam intensity $\Delta I/I$ were <1.4% for electrons and 2–4% for positrons, where I refers to $\ln(I_g/I_v)$ in Eq. (1). That of the gas density, $\Delta n/n$, was less than 1% for CH_3Cl and CH_3Br, and 2% for CH_3I which was in liquid form, while that due to the effective length of the collision cell $\Delta l/l$ was 2% for both projectiles. The purity of the CH_3X gases was better than 98%. The CH_3I gas molecules are highly reactive to direct light so that even though we did put a tight light shield, slight decomposition of this molecule may have taken place.

B. Theoretical model

The theoretical approach employed is the continuum multiple-scattering (CMS) method, which is a simple but efficient model for treating electron scattering from polyatomic molecules.[14] In short, to overcome difficulties arising from (i) the many degrees of freedom of electronic and nuclear motions and (ii) the nonspherical molecular field in polyatomic molecules, the CMS divides the configuration space into three regions: Region I, the atomic region surrounding each atomic sphere (spherical potentials), Region II, the interstitial region (a constant potential), and Region III, the outer region surrounding the molecule (a spherical potential). The scattering part of the method is based on the static-exchange-polarization potential model within the fixed-nuclei approximation. The static interaction is constructed with the electron density obtained from the CMS wave function, and the Hara-type free-electron gas model[14] is employed for the local-exchange interaction, while the dipole interaction is considered for terms only proportional to r^{-2}. A simple local exchange potential replaces the cumbersome nonlocal exchange potential making the calculations tractable.

Under these assumptions, the Schrödinger equation in each region is solved numerically under separate boundary conditions. By matching the wave functions and their derivatives from each region, we can determine the total wave functions of the scattered electron and hence, the scattering S-matrix. Once the S-matrix is obtained, the scattering cross section can be easily calculated by a conventional procedure. This CMS approach has been tested extensively and is known to provide useful information on the underlying scat-

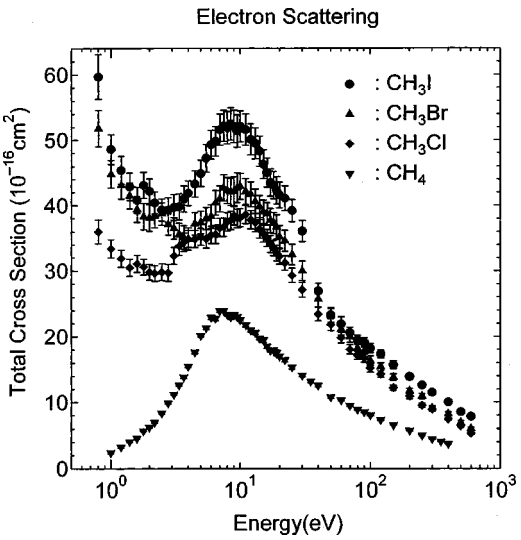

FIG. 2. Electron scattering TCSs for all CH_4, CH_3Cl, CH_3Br, and CH_3I molecules.

tering physics.[15] Further, the CMS method is useful for interpolation and extrapolation for guiding experimental data points.

III. RESULTS AND DISCUSSIONS

We discuss TCSs for electron and positron impact separately below. Furthermore, a detailed comparison with the CH_4 molecule is attempted for a better understanding of spectroscopic as well as dynamical aspects of these molecules.

A. Electron impact

TCSs for electron scattering from CH_3X (X=Cl, Br, and I) molecules are measured at energies in the range from 0.8 to 600 eV and shown for all molecules in Fig. 2, while TCSs for individual molecules are displayed in Figs. 3(a)–3(c). In Figs. 3(a)–3(c) previous experimental results[4–6] are also included. First we discuss the cross sections shown in Fig. 2, and then proceed to the results for the individual cases in Figs. 3(a)–3(c). The earlier results for CH_4 (Ref. 16) are also included in the figure for later discussion.

A few interesting general features of the present TCSs for all molecules are as follows: (i) The TCSs have a conspicuously large peak at around 10 eV, and drop rather sharply on the higher energy side. The magnitude of this peak decreases in the order of I→Br→Cl→H, i.e., the atomic size. (ii) The second smaller peak, which appears around at 4 eV for the Cl atom, shifts toward smaller energies for the Br atom at 2.5 eV and the I atom at 1.8 eV. (iii) Below ~1.5 eV, the TCSs turn around and begin to increase at much lower energies. This is a characteristic feature of polar molecules. (iv) A small shoulder emerges for all molecular species around 25–30 eV, but it is more pronounced for CH_3I.

The origin of the peak seen at around 2–4 eV has been well studied,[17] and is considered to be due to the formation of electron-attached anion states. The C–X (X=Cl, Br, and

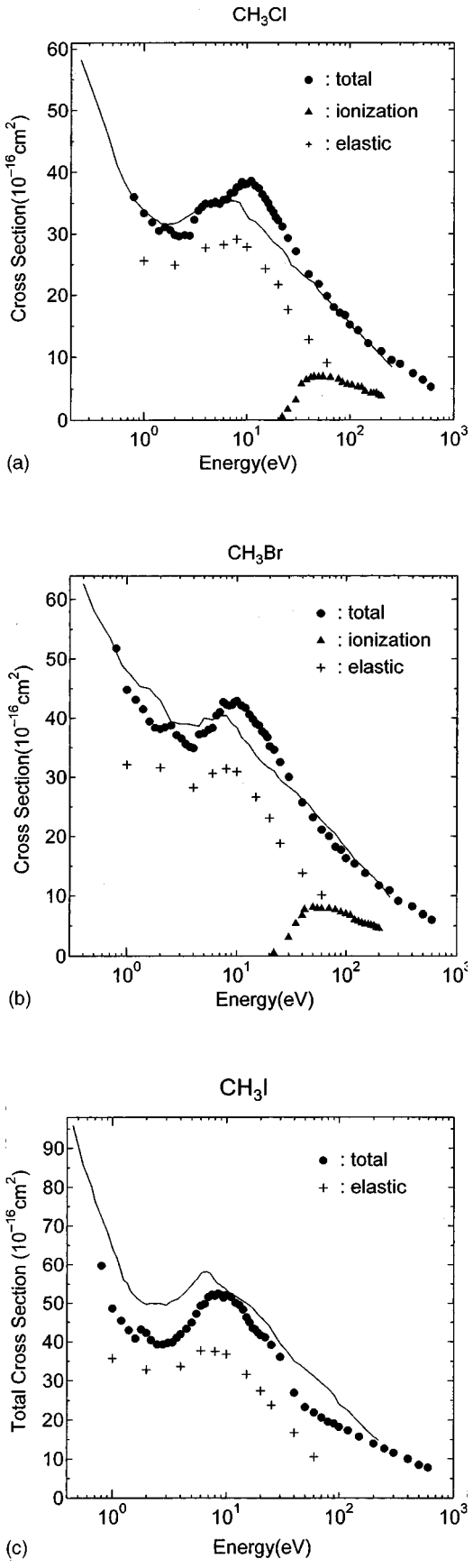

FIG. 3. TCSs for each molecule (a) CH_3Cl, (b) CH_3Br, and (c) CH_3I. Ionization cross sections (▲), and elastic cross sections (+) are also included in each panel. The experimental results by Krzysztofowicz and Szmytkowski (Ref. 5) are shown in a solid line.

TABLE II. LUMO, HOMO energies. All energies are in units of eV.

	CH_4[a]	Symmetry	CH_3Cl[b]	Symmetry	CH_3Br[c]	Symmetry	CH_3I[c]	Symmetry
LUMO[d]	3.54	a1	3.3	a1	2.1	a1	1.4	a1
HOMO	−14.3	t2	−11.3	e	−10.5	e	−9.5	e
OMOs	−25.7	a1	−14.4	a1	−13.5	a1	−12.5	a1
	⋯	⋯	−15.5	e	−15.1	e	−14.8	e

[a]Reference 19.
[b]Reference 17.
[c]Reference 18.
[d]All LUMOs are from Ref. 27.

I) σ^* orbitals are responsible for the resonances at this energy as well as those near 8 eV.

We have carried out a study of electronic states of the molecules, and phase shifts and eigenphase sum from scattering to identify positions and nature of resonances by the CMS. Our calculation suggests that the two lowest unoccupied molecular orbitals (LUMO) for CH_3Cl lie at 3.67 eV and 9.82 eV and are of a_1 symmetry. These values are in reasonable accord with previous experimental results.[17–19] Also our calculations show that these LUMO values shift to lower energies as the halogen atom becomes larger from Cl to I atoms, which is also consistent with the experiment as exemplified in Table II. These LUMOs together with higher ones are considered to be responsible for a larger peak at around 6–10 eV. Above approximately 15 eV, the small structure seen around 25 eV is due to the combination of $1a_1$ and $2a_1$ LUMOs.

As seen, the dominant peak shifts toward higher energies from 7 to 10 eV as a halogen atom becomes lighter from CH_3I to CH_3Cl. In contrast, the second weaker peak seen around 1.5–3 eV moves toward lower energies from 3.5 eV to 2 eV and then 1.6 eV as a halogen atom becomes heavier from CH_3Cl to CH_3Br and CH_3I. This is a clear manifestation of the shift of the energy levels of LUMOs as in Table II. At lower energies below the second peak, the TCSs begin to increase again. As described earlier, this feature is typical of polar molecules. Above ~100 eV, all TCSs decrease almost at the same rate, and the order of the magnitude of TCS is roughly proportional to the size of halogen atom. This is the region where the additivity rule within the Born approach may be able to provide a rough estimate of the TCS although its validity is still not clear.

Figures 3(a)–3(c) include the ionization cross sections of Ref. 9 for CH_3Cl and CH_3Br. Ionization is expected to become dominant above a few tens of eV, and hence constitutes a major part of the total cross section. The difference between the total and ionization cross sections furnishes information on the sum of elastic and other inelastic contributions. Among all inelastic processes, ionization and electronic excitation should predominantly become the primary process above 100 eV energy domain. Zecca *et al.*[20] reported on the partitioning of the total cross section for CH_4 that at 200 eV, elastic cross sections amount to about 40%, ionization to about 50%, and electronic excitation to about 5% of the total cross section, and the rest may come from rovibrational excitation. Although this number for electronic excitation appears to be too low, nevertheless we make a rough estimation for the partitioning for the present TCSs for all molecules based on their numbers. At 100 eV, for CH_3Cl, the ionization cross section can be read graphically as approximately $5.7\times10^{-16}\,cm^2$, which can be compared to the TCS value of $1.5\times10^{-15}\,cm^2$, i.e., the difference is roughly $9.3\times10^{-16}\,cm^2$, or about 40% of the total. At this energy, the contribution from elastic is expected to consist of 40–50% of the total, and therefore, the sum of all electronic excitation is considered to fill the gap of 10% or so. Hence, one could roughly estimate that the sum of all electronic excitation cross sections would be $3-4\times10^{-16}\,cm^2$. The differences between the respective TCS and ionization cross sections for the other two cases amount to approximately 3.2×10^{-16}, and $8.5\times10^{-16}\,cm^2$, for CH_4, and CH_3Br, respectively, at 100 eV, and as before, nearly 10% of these may correspond to the contribution from the sum of all electronic excitation processes. In the energy region between electronic excitation and ionization thresholds, at 10 eV for CH_3Cl, for example, the TCS is approximately $3.8\times10^{-15}\,cm^2$, while elastic cross sections amount to about $2.7\times10^{-15}\,cm^2$. And the difference of $1.1\times10^{-15}\,cm^2$ should come from the sum of electronic excitation and rovibrational excitation, in which each may share a half of the rest. In this energy domain, dissociative electron attachment (DEA) becomes possible. And in fact this process becomes a primary contributor to TCS when there is a resonance. We will discuss more about the DEA below. Below electronic excitation threshold, the TCS constitutes from elastic and rovibrational excitation as well as DEA. As discussed, the DEA often associates with a resonance having a sharp narrow peak, and if this is the case, the partitioning of the TCS cannot be done easily unless one has a reasonable information of the DEA cross section.

Elastic cross sections obtained by the CMS are also shown in Figs. 3(a)–3(c). The general energy dependence of the cross sections is similar to the TCSs, but the magnitude is 20–30% smaller than the TCS. The effect of the two peaks seen in the TCSs due to the resonances at ~3 and ~8 eV appear to be somewhat weaker in the elastic cross sections, and at the higher energy side above 20 eV, they decrease at a much higher rate than TCSs reflecting the growing importance of inelastic channels. Below approximately 10 eV, the difference between the TCS and elastic cross section should primarily come from rovibrational excitation and attachment. At 100 eV, the present elastic cross section amounts to 4.5×10^{-16}, 5.1×10^{-16}, and $5.4\times10^{-16}\,cm^2$ for CH_3Cl, CH_3Br, and CH_3I, respectively. These values for CH_3Cl and CH_3Br are slightly smaller than corresponding

ionization cross sections, but are nearly comparable. Hence, the sum of elastic and ionization cross sections constitutes approximately 75–80% of the respective total cross section, while other processes such as electronic excitation contribute the remaining. This distribution of various contributions to the total cross section appears to be reasonable.

B. Comparison with other measurements

The earlier TCSs for these molecules of Krzysztofowicz and Szmytkowski[4–6] are shown in Figs. 3(a)–3(c) for the comparison. Generally, the magnitude as well as the energy-dependence of the present TCSs for these three molecules are found to be in fair accord with earlier measurements. Particularly the magnitude of the present TCSs are very close to those of Krzysztofowicz and Szmytkowski[5,6] for CH_3Cl and for CH_3Br above 30 eV. However, the small but non-negligible deviation begins to emerge below this energy, and at the peak region around 10 eV, the present values are larger by 15%, at most, than those of Krzysztofowicz and Szmytkowski for both molecules. For CH_3I, the present TCSs are smaller by 10–15% than those of Krzysztofowicz and Szmytkowski[5,6] and Benitez *et al.*[7] in the entire energy range studied, although they begin to approach our values above 200 eV. For all molecules, it appears that the maximum values seen in the present TCSs at 10 eV are lower by 1–2 eV in the data of Krzysztofowicz and Szmytkowski. Benitez *et al.*[7] did not report TCSs for the energy region above 8 eV for all molecules, but their TCSs show a monotonically increasing trend in this energy range. Above the high-energy side of 75 eV, TCSs for CH_3Cl of Karwasz *et al.*[8] are found to be larger by 15% than the present TCSs. As for resonance structures, the present 10 eV dominant peak is clearly seen as being the sum of two small separate peaks at around 8 eV and 10 eV, while they are not clearly discriminated in previous experiments. As described below, this separation is important for providing detailed information of electronic structures. In addition, a small structure seen at 1.5 eV for CH_3Cl is also missing in the previous experiments although the one for CH_3Br at 2 eV appears to be present at much lower energy in the previous measurements.[5,6]

In the low-energy side below 10 eV, formation of Cl^-, Br^-, and I^- anions through DEA to CH_3Cl, CH_3Br, and CH_3I have been investigated.[21,22] The cross section for Cl^- formation from CH_3Cl shows two narrow peaks at 0.8 and 7.4 eV with magnitudes of approximately 2×10^{-21} and $5\times10^{-20}\,cm^2$, respectively.[21] A further contribution to the yield of Cl^- and CH_2Cl^- from CH_3Cl is found at about 7.4 eV and has been ascribed to DEA to higher-lying electronic states of CH_3Cl^-.[21] Although the appearance of peaks due to Br^- from CH_3Br at 0.35, 6.9, and 9.4 eV and I^- from CH_3I at 0.15 eV was found earlier, the magnitude for these DEA cross sections has not been reported.[22] The electron attachment cross section for CH_3Br was measured[23] based on swarm techniques, and the maximum value of the cross section for Br^- production was found to reach $1.8\times10^{-18}\,cm^2$ at around 0.4 eV. These DEA cross sections are smaller by at least two orders of magnitude than TCSs in general. This small cross section may be attributable to the ground vibrational state of parent molecules where the ground state potential may energetically separate from that of the dissociation channel. If they are in vibrationally excited states, then DEA cross section is expected to increase two-three orders of magnitude.[24] Therefore, the contribution from DEA processes to TCSs for each molecule is considered to be secondary in size, but certainly the understanding of its mechanism is an important subject which warrants a thorough study.

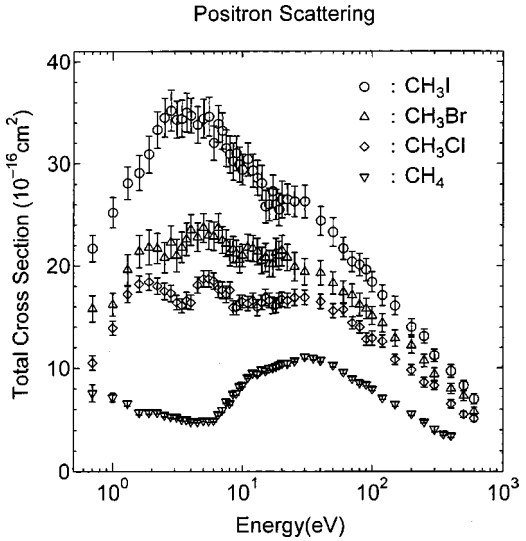

FIG. 4. Positron scattering total cross sections for all CH_4, CH_3Cl, CH_3Br, and CH_3I molecules.

Finally for CH_3Cl, the elastic and vibrational-excitation differential cross sections at 0.5–9 eV were measured by Shi *et al.*,[25] and seen to display the conspicuous forward peak arising from the nature of a polar molecule. They have estimated the total vibrational excitation cross section to be about $2.96\times10^{-16}\,cm^2$ at 3.2 eV, and reasoned that the resonance-like structure is due to the $^2A_1$ configuration of the ground state of the CH_3Cl^- ion. This vibrational excitation cross section constitutes about 10% of our TCSs. However, when they evaluated the vibrational excitation cross section at 1 eV, their value came out to be about $74\times10^{-16}\,cm^2$, which is twice as large as our and other TCSs at this energy.

Thresholds (of approximately 7.9, 6.2, and 4.7 eV, respectively) for electronic excitations for the $n\rightarrow\sigma^*$ transition of CH_3Cl, CH_3Br, and CH_3I molecules were measured using the photoabsorption spectroscopy.[26] These electronic excited states are unstable and eventually dissociate producing ground-state or excited halogen atom and methyl radicals. Appearance potentials for various fragmented ions and radicals for these molecules are not well studied. This is an important research area since information on fragmentation of molecules is extremely important for various applications. Electronic orbital energies[17–19,27] are listed in Table II.

C. Positron Impact

TCSs for positron impact for the three molecules are displayed in Fig. 4 along with those for CH_4.[16] A few remarks on the TCSs are warranted: (i) Positronium (Ps) formation thresholds are 4.42 eV, 3.74 eV, and 2.738 eV for CH_3Cl, CH_3Br, and CH_3I, respectively, and at corresponding energies, small peaks due to this formation can be seen; (ii)

small structures above 10 eV are due to the opening of ionization channels; (iii) between Ps formation and ionization thresholds, some weak structures due to electronic excitation are also visible; (iv) a conspicuous peak is apparent at slightly below 2 eV for all molecules; and (v) the cross sections begin to drop rather sharply below 1–3 eV. Although the origin of the peak at 2 eV is not known, it may well be contributions from rovibrational excitation, or positron attachment. The reason for the sharp drop of TCSs below this peak is not also clear, and somewhat puzzling as discussed below. Except for CH_3I, the dipole moments for the other two molecules are slightly larger than 1.625 D; the critical dipole moment which enables support for an infinite number of electron or positron bound states.[28] Therefore, CH_3Cl and CH_3Br can easily form a bound state with a positron. The structure at around 2 eV for CH_3Cl and CH_3Br is much stronger and is clearly visible while that for CH_3I is weak, but is present. And for CH_4, a nonpolar molecule, there is no hint of any structure in this energy region.[16] Hence, this stronger structure for CH_3Cl and CH_3Br is suggestive of a binding state.

In the present entire impact-energy range, the TCSs for positrons are found to be always smaller than those for electrons. This situation is different compared to the case of CO_2,[29] where the magnitude of the TCS for electron and positron impact reverse in the energy between 3 and 0.8 eV and the electron TCSs become larger again below 0.8 eV. We have tentatively argued that this reversal is due to larger rotational excitation cross sections for positron impact for CO_2, although certainly, the possibility of resonance formation due to positron attachment cannot be excluded. Other weak structures can also be seen throughout the entire energy range. However the origin of these structures is also not well understood, and certainly the possibility of resonance formation exists. It is very interesting to compare the present TCSs with those for CH_4. For CH_4, the TCSs show conspicuously a large peak centered at around 30 eV, and at both sides of this energy, the TCSs decrease smoothly. Halogenization would certainly give a strong effect.

D. A comparison of TCSs between electron and positron impacts

Both TCSs for electron and positron impacts on all molecules by the present results only are plotted in Figs. 5(a)–5(c). As a general trend for all molecules, TCSs for electron and positron appear to merge reasonably well beyond a few hundred of eV. At low-to-intermediate energies, the TCSs for electron impact are always larger by nearly a factor of two due to resonances over the 3–30 eV region. This characteristic is a clear reflection of differences in the interaction between the electron and positron with molecules. Below 3 eV, the TCSs for electron impact show a sharply increasing trend, while TCSs for positron impact display an opposite trend, i.e., a sharply decreasing trend. This low energy behavior in the two TCSs is a very sharp contrast. The TCSs for both should rise at low energies because of the strong dipole moments, and if this long-range dipole interaction dominates, then the two sets of TCSs should behave simi-

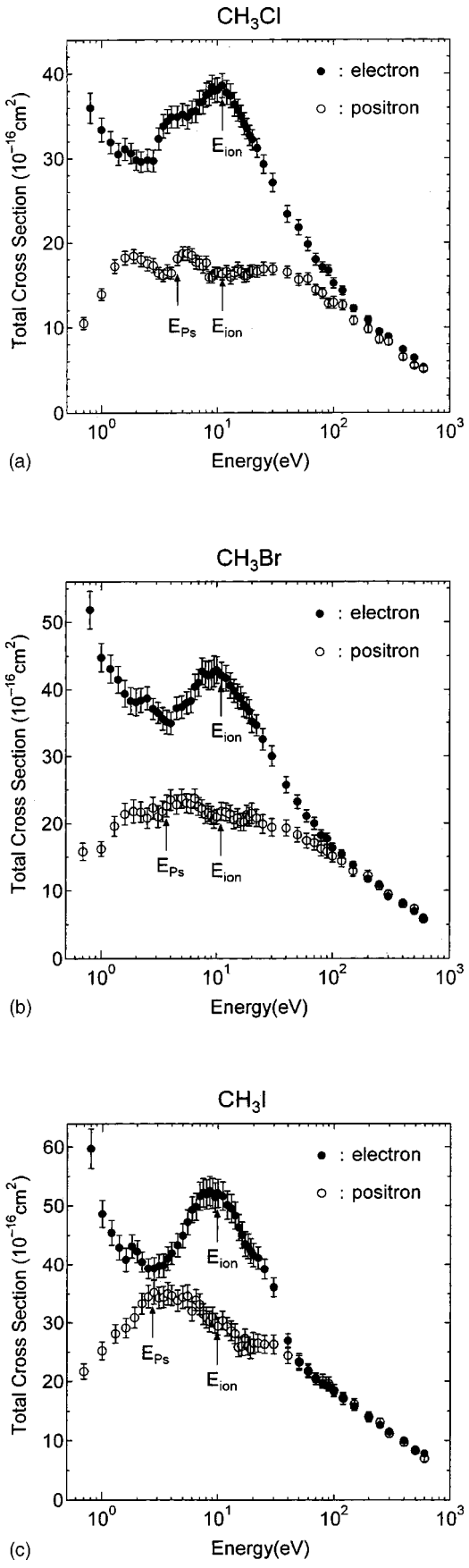

FIG. 5. Comparison in the total cross sections by electron (full circles) and positron (open circles) scattering for the individual molecule, (a) CH_3Cl, (b) CH_3Br, and (c) CH_3I. The E_{ion} and E_{Ps} with the vertical arrow indicate the threshold of the ionization and the positronium formation for each molecule, respectively.

TABLE III. (a) The TCSs(10^{-16} cm^2) of electron impacts. (b) The TCSs(10^{-16} cm^2) of position impacts.

	eV	CH_3Cl	CH_3Br	CH_3I		eV	CH_3Cl	CH_3Br	CH_3I
(a)	0.8	36.0±1.8	51.8±2.8	59.7±3.4		600	5.3±0.2	6.0±0.2	7.8±0.3
	1.0	33.4±1.4	44.8±2.1	48.6±2.3	(b)	0.7	10.5±0.7	15.8±1.3	21.7±1.3
	1.2	31.9±1.3	43.1±2.1	45.4±2.1		1.0	13.9±0.7	16.2±1.1	25.2±1.5
	1.4	30.5±1.3	41.5±2.0	42.9±2.1		1.3	17.2±0.8	19.6±1.5	28.1±1.6
	1.6	31.1±1.3	39.4±2.0	40.8±2.0		1.6	18.2±0.8	21.4±1.7	29.1±1.7
	1.8	30.6±1.2	38.3±2.0	43.1±2.0		1.9	18.4±0.8	21.8±1.7	30.9±1.8
	2.0	29.8±1.2	38.1±2.0	42.2±1.9		2.2	18.0±0.8	21.7±1.5	33.3±1.8
	2.2	29.6±1.2	38.4±1.7	40.4±1.7		2.5	17.5±0.8	20.8±1.5	34.5±1.9
	2.5	29.8±1.3	38.7±1.7	39.3±1.7		2.8	17.3±0.8	22.3±1.6	35.2±2.0
	2.8	29.7±1.3	37.1±1.6	39.3±1.9		3.1	16.4±0.7	21.0±1.6	34.3±1.8
	3.1	32.3±1.3	36.5±1.6	39.7±2.0		3.4	16.1±0.7	21.8±1.5	34.4±1.8
	3.4	33.8±1.4	35.6±1.7	39.8±2.0		3.7	16.6±0.8	22.6±1.6	39.7±2.0
	3.7	34.4±1.4	35.6±1.8	41.0±2.0		4.0	16.4±0.7	23.5±1.5	34.7±1.7
	4.0	34.9±1.3	34.9±1.7	41.9±1.9		4.5	18.1±0.8	22.8±1.4	33.8±1.8
	4.5	34.9±1.3	37.2±1.7	43.3±2.0		5.0	18.7±0.8	23.7±1.4	34.4±1.9
	5.0	35.2±1.3	37.4±1.8	44.9±2.0		5.5	18.7±0.8	23.0±1.4	34.6±1.9
	5.5	34.9±1.4	38.0±1.7	47.2±2.1		6.0	18.5±0.8	22.9±1.4	32.0±1.7
	6.0	35.5±1.3	38.3±1.8	49.3±2.2		6.5	17.7±0.8	23.7±1.4	33.9±1.8
	6.5	35.6±1.4	40.4±1.9	49.8±2.3		7.0	17.6±0.8	22.5±1.3	33.2±1.8
	7.0	36.6±1.4	41.0±2.0	51.6±2.4		7.5	17.2±0.8	22.2±1.3	31.5±1.8
	7.5	36.7±1.4	42.7±2.0	52.2±2.4		8.0	17.6±0.8	21.3±1.3	30.9±1.8
	8.0	37.5±1.4	42.3±2.0	51.9±2.5		8.5	15.9±0.7	21.6±1.3	30.2±1.8
	8.5	37.7±1.4	42.1±2.1	52.5±2.5		9.0	15.9±0.7	21.2±1.3	31.0±1.7
	9.0	38.4±1.4	42.2±2.2	51.4±2.5		9.5	16.4±0.7	20.6±1.3	29.9±1.7
	9.5	38.0±1.4	42.7±2.3	51.4±2.5		10	16.5±0.6	21.0±1.1	29.4±1.5
	10	38.1±1.4	42.9±2.0	52.1±2.4		11	16.3±0.7	21.8±1.3	31.4±1.6
	11	39.6±1.4	42.1±2.0	51.6±2.4		12	16.6±0.7	21.7±1.3	29.3±1.6
	12	37.8±1.4	41.7±1.9	50.1±2.4		13	15.9±0.8	21.4±1.3	28.6±1.7
	13	37.4±1.4	40.6±1.9	49.5±2.4		14	16.4±0.7	20.5±1.4	28.1±1.7
	14	36.4±1.4	39.8±1.7	48.3±2.3		15	16.9±0.8	20.8±1.4	25.8±1.6
	15	35.7±1.3	39.0±1.8	46.3±2.2		16	16.6±0.7	20.2±1.3	26.0±1.6
	16	35.0±1.3	38.7±1.7	45.0±2.2		17	16.1±0.8	20.2±1.3	27.3±1.6
	17	34.1±1.3	37.7±1.8	43.5±2.1		18	16.1±0.7	21.3±1.4	26.0±1.5
	18	33.5±1.2	37.3±1.6	43.1±2.1		19	16.6±0.7	21.0±1.4	25.5±1.8
	19	32.7±1.2	36.7±1.8	42.3±2.1		20	16.7±0.7	21.5±1.5	26.5±1.8
	20	32.2±1.2	35.2±1.7	41.6±2.0		22	16.6±0.8	20.8±1.3	26.5±1.5
	22	31.2±1.1	34.6±1.6	41.1±1.9		25	16.9±0.8	19.9±1.4	26.3±1.5
	25	31.2±1.1	32.5±1.6	39.2±1.7		30	16.9±0.7	19.4±1.3	26.3±1.6
	30	27.1±1.1	30.0±1.5	36.1±1.6		40	16.5±0.7	19.3±1.2	24.4±1.4
	40	23.4±1.0	25.7±1.2	26.9±1.2		50	15.6±0.7	18.3±1.1	23.3±1.4
	50	21.8±0.9	23.2±1.0	23.3±1.1		60	15.7±0.7	17.4±1.1	21.7±1.1
	60	19.8±0.8	21.1±0.9	21.9±1.1		70	14.4±0.6	17.1±1.1	20.4±1.0
	70	18.0±0.7	20.0±0.9	20.6±0.8		80	14.0±0.6	16.2±1.1	20.1±1.1
	80	17.1±0.6	18.2±0.8	19.5±0.7		90	12.8±0.6	15.8±1.0	19.6±1.1
	90	16.7±0.6	17.7±0.8	19.1±0.7		100	12.9±0.7	15.1±0.9	18.4±1.0
	100	15.2±0.6	16.3±0.7	18.2±0.7		120	12.6±0.6	14.4±0.9	17.1±1.0
	120	14.3±0.5	15.4±0.6	17.3±0.6		150	10.8±0.5	12.9±0.8	16.1±0.9
	150	12.2±0.4	13.8±0.5	15.7±0.6		200	9.8±0.5	12.2±0.8	14.0±0.8
	200	10.9±0.4	11.7±0.4	13.9±0.5		250	8.6±0.5	10.7±0.6	13.1±0.7
	250	9.5±0.3	10.9±0.4	12.6±0.4		300	8.3±0.4	9.4±0.6	11.2±0.6
	300	8.9±0.3	9.1±0.3	11.5±0.4		400	6.5±0.4	8.0±0.5	9.7±0.6
	400	7.4±0.2	8.2±0.3	8.5±0.4		500	5.5±0.3	7.3±0.5	8.3±0.5
	500	6.4±0.2	6.9±0.3	8.5±0.3		600	5.1±0.1	5.8±0.4	7.0±0.5

larly at these low energies. However, in our experiments, only the TCSs for electron impact show behavior characteristic of polar molecules in the energy range. This clearly suggests that a short-range interaction that is different for electron and positron impact still significantly contributes to scattering dynamics, resulting in a different behavior in the two TCSs. This raises an interesting and important question: At what energy do positron-TCSs turn around, and why is this energy different from that for electron-TCSs. The answer to this should provide us with more basic knowledge of the interaction between the two projectiles.

Numerical data for all cross sections both for electron and positron impacts are listed in Table III.

IV. SUMMARY

In this paper, we present the experimental TCSs for CH_3Cl, CH_3Br, and CH_3I molecules by electron and positron impacts from 0.7 to 600 eV. All the TCSs for electron im-

pacts are found to be in reasonably good accord with other earlier measurements. The theoretical elastic cross section is calculated using the CMS method, and this method is also employed to carry out the analysis of the molecular structures of these molecules so as to identify the origin of resonances. This analysis provides reasonable rationales to the general shape and magnitude of all TCSs and resonance structures by electron impact. We discuss the present resonance structures in relation to the previous results for dissociative electron attachment. We observe an interesting difference in the low energy TCSs between electron and positron impacts. Below ~2 eV, electron-TCSs show an increasing trend, while positron TCSs drop sharply. This demonstrates a strong manifestation of molecular size effects on TCSs. This difference may be attributable to the role of a short-range interaction. However more detailed and comprehensive understanding should await for more thorough joint theoretical and experimental investigation.

ACKNOWLEDGMENT

The work was supported in part by the Grant-in-Aid, the Ministry of Education, Science, Technology, Sport, and Culture, Japan (M.K.).

[1] L. G. Christophorou, *Electron–Molecules Interactions and their Applications* (Academic, New York, 1984), Vols. I and II.
[2] M. Kimura, O. Sueoka, A. Hamada, and Y. Itikawa, Adv. Chem. Phys. **111**, 537 (2000).
[3] M. K. Kawada, O. Sueoka, and M. Kimura, Chem. Phys. Lett. **330**, 34 (2000).
[4] C. Szmytkowski and A. M. Krzysztofowicz, Chem. Phys. Lett. **209**, 474 (1993).
[5] A. M. Krzysztofowicz and C. Szmytkowski, Chem. Phys. Lett. **219**, 86 (1994).
[6] A. M. Krzysztofowicz and C. Szmytkowski, J. Phys. B **28**, 1593 (1995).
[7] A. Benitez, J. H. Moore, and J. A. Tossell, J. Chem. Phys. **88**, 6691 (1988).
[8] G. P. Karwasz, R. S. Brusa, A. Piazza, and A. Zecca, Phys. Rev. A **59**, 1341 (1999).
[9] C. Vallance, S. A. Harris, J. E. Hudson, and P. W. Harland, J. Phys. B **30**, 2465 (1997).
[10] P. D. Burrow, A. Modelli, and N. S. Chiu, J. Chem. Phys. **77**, 2699 (1982).
[11] O. Sueoka, S. Mori, and A. Hamada, J. Phys. B **27**, 1453 (1994).
[12] K. R. Hoffman, M. S. Dababneh, Y.-F. Hsieh, W. E. Kauppila, V. Pol, J. H. Smart, and T. S. Stein, Phys. Rev. A **25**, 1393 (1982).
[13] A. Hamada and O. Sueoka, J. Phys. B **27**, 5055 (1994).
[14] M. Kimura and H. Sato, Comments At. Mol. Phys. **26**, 333 (1991).
[15] H. Tanaka, Y. Tachibana, M. Kitajima, O. Sueoka, H. Takaki, A. Hamada, and M. Kimura, Phys. Rev. A **59**, 2006 (1999).
[16] O. Sueoka and S. Mori, J. Phys. B **19**, 4035 (1986).
[17] M. Guerra, D. Jones, G. Distefano, F. Scagnolari, and A. Modelli, J. Chem. Phys. **94**, 484 (1991).
[18] A. Modelli, F. Scagnolari, G. Distefano, D. Jones, and M. Guerra, J. Chem. Phys. **96**, 2061 (1992).
[19] Y. H. Kim, M. Stadele, and R. M. Martin, Phys. Rev. A **60**, 3633 (1999).
[20] A. Zecca, G. P. Karwasz, and R. Brusa, Phys. Rev. A **45**, 2777 (1992).
[21] D. M. Pearl and P. D. Burrow, J. Chem. Phys. **101**, 2940 (1994).
[22] J. A. Stockdale, F. J. Davis, R. N. Compton, and C. E. Klots, J. Chem. Phys. **60**, 4279 (1974).
[23] P. G. Datskos, L. G. Christophorou, and J. G. Carter, J. Chem. Phys. **97**, 9031 (1992).
[24] M. Kimura, in *Adv. At. Mol. Opt. Phys.*, edited by M. Kimura and Y. Itikawa (Academic, New York, 2001), Vol. 44, p. 33.
[25] X. Shi, V. K. Chan, G. A. Gallup, and P. D. Burrow, J. Chem. Phys. **104**, 1855 (1996).
[26] M. B. Robin, Can. J. Chem. **63**, 2032 (1985).
[27] K. Kimura, *Handbook of He I Photoelectron Spectra of Fundamental Organic Molecules* (Japan Scientific Society, Tokyo, 1981).
[28] W. R. Garrett, J. Chem. Phys. **73**, 5721 (1980).
[29] M. Kimura, O. Sueoka, A. Hamada, M. Takekawa, Y. Itikawa, H. Tanaka, and L. Boesten, J. Chem. Phys. **107**, 6616 (1997).
[30] *CRC Handbook of Chemistry and Physics* (CRC, New York, 2000).